Determination of macroscopic transport coefficients of a dissipative particle dynamics solvent

Dmitrii Azarnykh,[1,*] Sergey Litvinov,[2] Xin Bian,[3] and Nikolaus A. Adams[1]
[1]*Institute of Aerodynamics and Fluid Mechanics, Technische Universität München, Garching, Germany*
[2]*Chair for Computational Science, Eidgenössische Technische Hochschule Zürich, Zurich, Switzerland*
[3]*Division of Applied Mathematics, Brown University, Providence, Rhode Island 02912, USA*
(Received 30 September 2015; revised manuscript received 15 December 2015; published 11 January 2016)

We present an approach to determine macroscopic transport coefficients of a dissipative particle dynamics (DPD) solvent. Shear viscosity, isothermal speed of sound, and bulk viscosity result from DPD-model input parameters and can be determined only *a posteriori*. For this reason approximate predictions of these quantities are desirable in order to set appropriate DPD input parameters. For the purpose of deriving an improved approximate prediction we analyze the autocorrelation of shear and longitudinal modes in Fourier space of a DPD solvent for Kolmogorov flow. We propose a fitting function with nonexponential properties which gives a good approximation to these autocorrelation functions. Given this fitting function we improve significantly the capability of *a priori* determination of macroscopic solvent transport coefficients in comparison to previously used exponential fitting functions.

DOI: 10.1103/PhysRevE.93.013302

I. INTRODUCTION

The dissipative particle dynamics (DPD) method is a stochastic numerical model for the representation of mesoscale phenomena in fluids. It was first suggested by Hoogerbrugge and Koelman [1]. DPD is widely applied in physics and engineering science. It has been used for, among others, modeling of polymer solutions [2], red blood cells [3], and colloidal suspensions [4,5]. One of the main complications of the DPD method lies in determining effective macroscopic fluid coefficients, such as viscosity and compressibility. Such macroscopic transport coefficients are indirectly determined by a set of DPD input parameters which are essentially of microscopic nature. A relation between DPD and molecular dynamics with Lennard-Jones potential was demonstrated in [6]. In contrast to DPD, smoothed dissipative particle dynamics (SDPD) has an inherently macroscopic nature, and macroscopic transport coefficients characterized by shear and bulk viscosities and isothermal speed of sound have a direct correspondence to SDPD input parameters. SDPD was first proposed in [7] as a stochastic extension of the smoothed particle hydrodynamics (SPH) method to the mesoscale [8]. For that reason SDPD is limited to the classical hydrodynamic regime of fluids, where macroscopic transport coefficients do not depend on length scales. It should be pointed out that the SDPD model and the Landau-Lifshitz Navier-Stokes (LLNS) equations are related to each other for certain input-parameter ranges [9]. As SDPD and LLNS are limited to the classical hydrodynamic regime, the challenge of finding a relation between macroscopic and DPD input parameters cannot be solved through modeling a DPD solvent with SDPD or LLNS. A variety of methods have been proposed to estimate macroscopic transport coefficients for a DPD solvent. The common approach is to expose a DPD solvent to a body force which is constant in time. The shear viscosity can then be derived directly from the response of the solvent to such a perturbation. Fan *et al.* [10] used wall-bounded Poiseuille flow to asses the viscosity of a DPD solvent in a microchannel. A constant body force was applied in the wall-parallel direction, and the channel walls were modeled as frozen solvent particles. The same method was used to estimate the viscosity of a polymer suspension in a microchannel. It is also possible to estimate the viscosity of a DPD solvent by using a reverse Poiseuille flow [11–13], which implies the application of equal body forces with opposite direction in each half of the periodic domain. Another approach to estimate shear viscosity is to employ the Green-Kubo method which can lead to inaccuracies at small scales and may require additional corrections [14]. The Green-Kubo method as well as Poiseuille flow allow us to estimate the shear viscosity only on the length scale which is predefined by the initial conditions. If the shear viscosity does not depend on the length scale, as is the case for the Navier-Stokes equations, this approach is sufficient to predict dissipation on the different length scales. However, a DPD solvent has a more complicated relation between dissipation and length scales which is defined by the DPD weighting function and DPD dissipation as well as the repulsive potential. Another limitation is that stationary Poiseuille flow methods are unable to predict other macroscopic transport coefficients such as the bulk viscosity of a DPD solvent or its isothermal speed of sound. The dissipation in a DPD solvent without potential was widely analyzed in the classical works on DPD [15–17]. Predictions for the length scale dependency of macroscopic transport coefficients have been derived analytically from the DPD Fokker-Planck equation. In the analytical derivation of macroscopic transport coefficients some assumptions were imposed such as the absence of a potential between DPD particles. The main disadvantage of a DPD fluid without conservative force is due to the fact that the equation of state of such a fluid becomes that of an ideal gas [17]. It thus limits the model applicability. In [17] it was suggested to estimate macroscopic transport coefficients of a DPD solvent from the approximation of the Fourier transform of the velocity autocorrelation functions (FTVACF) with an exponential function. The approximation of FTVACF modes with an exponential function might introduce additional errors in the

*d.azarnykh@tum.de

estimation of shear viscosity [11]. It was demonstrated that when FTVACF modes are exponential (in the limit of long time and large length scale $\omega \to 0, k \to 0$) the viscosity estimated with the Green-Kubo method equals that estimated from the first FTVACF mode [14,20]. In principle one can consider the Green-Kubo method as a particular case of the more general FTVACF analysis. In this work we consider a DPD solvent with repulsive potential and show that an assumption of exponential decay of FTVACF modes implies additional errors in the estimation of macroscopic transport coefficients for a DPD solvent. The estimation of viscosity from FTVACF modes is well established for particle methods. The analysis of FTVACF in a multiparticle collision dynamics (MPC) solvent is described in [18], where an exponential function was used to estimate macroscopic transport coefficients of MPC. When the FTVACF-mode decay is not purely exponential, it may be useful to introduce a so-called memory function. Palmer [14] analyzed the transverse-current autocorrelation function for molecular dynamics with an exponential model of the memory function. The method also was compared with an estimate of the shear viscosity from Green-Kubo and Poiseuille flows for molecular dynamics [19]. Other models for the memory function are described in [20]. In this paper we analyze FTVACF modes of a DPD solvent in three spatial dimensions. We approximate the nonexponential evolution of FTVACF modes in a DPD solvent. For that purpose we introduce a function with nonexponential decay and calibrate its transport coefficients. This function gives a good approximation to the modes of FTVACF of a DPD solvent. We show that the analysis of FTVACF modes can be used to derive the wave-number dependence of the shear viscosity, the isothermal speed of sound, and the bulk viscosity of a DPD solvent. The paper is structured in the following way. After summarizing the DPD solvent model in the second section, we derive the shear viscosity on different scales from an analysis of Kolmogorov flows in the third section. In the fourth section we analyze the response of a DPD solvent on linear perturbations. We perform simulations for the decay of sinusoidal waves in longitudinal and transverse directions. For the case of sinusoidal wave decay we compare the maximum velocities at different wave numbers. In the same section the nonexponential nature of FTVACF is shown. We define the Fourier transform of the density autocorrelation function (FTDACF) to estimate the accuracy of prediction of macroscopic transport coefficients. We also introduce a function that improves the approximation of FTVACF modes of a DPD solvent in comparison with an exponential function. In the fifth section we compare the accuracy of the methods that can be used to derive macroscopic transport coefficients. We change the input parameters of the DPD solvent in the sixth section in order to assess applicability limits of the approach.

II. THE DPD METHOD

We consider a set of identical particles interacting with each other with a pairwise force F_{ij}. The law of motion for the ith particle is described by

$$\frac{d\boldsymbol{r}_i}{dt} = \boldsymbol{v}_i, \quad \frac{d\boldsymbol{v}_i}{dt} = \frac{1}{m}\sum_{j\neq i} \boldsymbol{F}_{ij}. \tag{1}$$

Here we take mass of the particle equal to unity. The force can be split into three parts:

$$\boldsymbol{F}_{ij} = \boldsymbol{F}^C_{ij} + \boldsymbol{F}^D_{ij} + \boldsymbol{F}^R_{ij}. \tag{2}$$

The pairwise forces have a cutoff radius r_c which we take as unity as well. The conservative force is repulsive between particles and acts along the connecting line between two particles:

$$\boldsymbol{F}^C_{ij} = \begin{cases} a_{ij} m(1 - r_{ij})\hat{\boldsymbol{r}}_{ij}, & r_{ij} < r_c \\ 0, & r_{ij} \geqslant r_c \end{cases}, \tag{3}$$

where a_{ij} is the maximum repulsion between the particles; $\boldsymbol{r}_{ij} = \boldsymbol{r}_i - \boldsymbol{r}_j$, $r_{ij} = |\boldsymbol{r}_{ij}|$, and $\hat{\boldsymbol{r}}_{ij} = \boldsymbol{r}_{ij}/r_{ij}$ are relative position, distance, and unit vector between two particles i and j, respectively. Dissipative and random forces are

$$\boldsymbol{F}^D_{ij} = -\gamma m w_D(r_{ij})(\hat{\boldsymbol{r}}_{ij} \cdot \boldsymbol{v}_{ij})\hat{\boldsymbol{r}}_{ij} \tag{4}$$

and

$$\boldsymbol{F}^R_{ij} = \sigma m w_R(r_{ij})\theta_{ij}\hat{\boldsymbol{r}}_{ij}, \tag{5}$$

respectively, where γ and σ are dissipative and random coefficients. $w^D(r_{ij})$ and $w^R(r_{ij})$ are weighting functions, $\boldsymbol{v}_{ij} = \boldsymbol{v}_i - \boldsymbol{v}_j$ is the relative velocity, and θ_{ij} is a random function with the properties

$$\langle \theta_{ij}(t) \rangle = 0, \tag{6}$$

$$\langle \theta_{ij}(t)\theta_{kl}(t') \rangle = (\delta_{ik}\delta_{jl} + \delta_{il}\delta_{jk})\delta(t - t'), \tag{7}$$

with $i \neq j$, $k \neq l$. The coefficients of the random and dissipative forces are related such that they satisfy the fluctuation-dissipation balance [21]

$$w^D(r_{ij}) = [w^R(r_{ij})]^2, \quad \gamma = \frac{\sigma^2}{2k_B T}, \tag{8}$$

where k_B is the Boltzmann constant and T is the temperature. We choose the standard weighting functions [2]

$$w^D(r_{ij}) = [w^R(r_{ij})]^2 = \begin{cases} (1 - r_{ij})^2, & r_{ij} < r_c \\ 0, & r_{ij} \geqslant r_c \end{cases}. \tag{9}$$

The velocity Verlet algorithm is used for time integration. Simulations in this work are performed with the LAMMPS open-source code [22].

Nondimensional transport coefficients

DPD can represent dynamics of a fluid in different scale regimes. On the large scales DPD obeys laws of classical hydrodynamics. On the small scales the dynamics of a DPD solvent differ from classical hydrodynamics. As scaling parameters that separate the dynamic regimes of a DPD solvent one may take a decorrelation length of DPD particles l_0 and the cutoff length r_c. Here we follow [17] and choose nondimensional transport coefficients as presented in Table I. We choose the mass of DPD particles m as a mass unit, the collision time t_0 as time unit, and the dynamic length l_0 as a length unit. We nondimensionalize transport coefficients such as kinematic shear viscosity, kinematic bulk viscosity, and isothermal speed of sound according to the chosen system of units. Nondimensional transport coefficients will be used in Sec. VI.

TABLE I. Scaling ratios for DPD nondimensional transport coefficients.

ν	Kinematic shear viscosity	$\nu = \frac{\eta_s}{\rho}$
ζ	Kinematic bulk viscosity	$\zeta = \frac{\eta_v}{\rho}$
v_0	Thermal velocity	$\sqrt{k_B T/m}$
$[\boldsymbol{r} w_D]_r$	Integral of w_D	$[\boldsymbol{r} w_D]_r = \int_0^{r_c} w_D(\boldsymbol{r}) d\boldsymbol{r}$
ω_0	Collision frequency	$\omega_0 = \rho [\boldsymbol{r} w_D]_r \gamma / d$
t_0	Collision time	$t_0 = \frac{1}{\omega_0}$
l_0	Dynamic distance	$l_0 = t_0 v_0$
Ω_0	Dynamic overlapping	$\Omega_0 = \frac{r_c}{l_0}$
$\tilde{k}$	Nondimensional wave number	$\tilde{k} = k l_0$
$\tilde{\nu}$	Nondimensional ν	$\tilde{\nu} = \frac{\nu}{\omega_0 l_0^2}$
$\tilde{\zeta}$	Nondimensional ζ	$\tilde{\zeta} = \frac{\zeta}{\omega_0 l_0^2}$
$\tilde{c}_t$	Nondimensional c_t	$\tilde{c}_t = \frac{c_t}{\omega_0 l_0}$

III. KOLMOGOROV FLOW OF SIMPLE DPD FLUID

One common approach to asses shear viscosity of a DPD system is to expose the DPD solvent to a temporally constant body force [10]. In this work we choose a sinusoidal spatial dependence for the body force that acts on the solvent. This particular choice of the force is motivated by convenience: sinusoidal waves have simple Fourier representations. We are interested in the low Reynolds number regime where nonlinear effects of the solvent are negligible. The choice of sinusoidal waves corresponds to the Kolmogorov-flow configuration which allows us to measure viscosity at any prescribed wave number [23,24]. We consider a body force

$$\boldsymbol{F} = F_0(k_z)\sin(k_z x)\hat{\boldsymbol{x}}, \tag{10}$$

where $k_z = 2\pi n/L_z$ is the z component of a wave-number vector, L_z is the extent of the simulation box in the z direction, n is an integer wave number, and $F_0(k_z)$ is a body force that depends on the wave-number vector in a way that will be described below. For small Reynolds number $\mathrm{Re} < \sqrt{2}$, one can obtain an analytical stationary solution

$$\boldsymbol{v} = v_0 \sin(k_z x)\hat{\boldsymbol{x}}, \tag{11}$$

with $v_0 = \frac{F_0(k_z)\rho}{m\eta_s k_z^2}$. The Reynolds number is defined as

$$\mathrm{Re} = \frac{F_0(k_z)}{m\nu^2 k_z^3}. \tag{12}$$

To estimate the viscosity law $\eta_s(k)$ we perform separate simulations for different k_z. For every simulation we take the body force $F_0(k_z)$ in such a way as to maintain $\mathrm{Re} \in [0.2, 0.3]$ for $L_z = 40$. An empirical expression for $F_0(k_z)$ is

$$F_0(k_z) = \begin{cases} 0.0199\, k_z^3, & k_z < \frac{2\pi\times 14}{40} \\ 0.00125\, k_z^2, & k_z \geqslant \frac{2\pi\times 14}{40} \end{cases}. \tag{13}$$

The simulation input parameters are described in Table II and are taken from [10]. To assess the shear viscosity, for every k_z we perform a preliminary simulation for a sufficiently long time until the Kolmogorov flow becomes stationary. Subsequently, for the developed stationary flow we evaluate

TABLE II. Input parameters of the DPD solvent for Kolmogorov flow.

Domain size ($L_x \times L_y \times L_z$)	$40 \times 40 \times 40$
Mass (m)	1
Temperature ($k_B T$)	1
Stochastic coefficient (σ)	3
Dissipative coefficient (γ)	$\sigma^2/(2k_B T)$
Repulsion coefficient (a_{ij})	18.75
Time step (dt)	0.01
Density (ρ)	4
Prerun length in time steps	4×10^5
Simulation length in time steps (N_t)	32×10^5

N_i samples from every simulation. Every sample represents an independent instantaneous velocity profile. We approximate each sample of the velocity profiles with a sinusoidal function (11) to extract the maximum velocity v_0. From the value of v_0 we estimate the shear viscosity η_s for every k_z. We find the statistical error of the shear viscosity estimation from the standard deviation of η_s. To achieve an error in viscosity estimation of less than 1%, we extend the simulation for the first integer wave number $n = 1$ up to $16 \times N_t$ time steps and for the second integer wave number $n = 2$ up to $8 \times N_t$ time steps, and so forth, where N_t is given in Table II. Figure 1 shows the velocity profiles averaged from N_i samples for $n = 1$ and 4. We consider the shear viscosity, estimated from Kolmogorov flow as a reference for the remainder of the paper. The viscosity law $\eta_s(k)$ which has been derived from this method is shown in Fig. 5.

IV. DPD RESPONSE ON LINEAR PERTURBATIONS

In this section we consider the linear response of a DPD solvent on perturbations. Such perturbations can be imposed by initial conditions in terms of longitudinal and transverse waves. Another option is to consider the transport and dissipation of equilibrium fluctuations. In the linear case the dissipation of random velocity fluctuations obeys the same dissipative evolution as the relaxation of an initially imposed velocity field. The correspondence of the two approaches was shown in [25] for fluctuating hydrodynamics. For a DPD solvent such a correspondence will be shown below. From the linear response of a DPD solvent one can derive the length scale dependence of macroscopic transport coefficients.

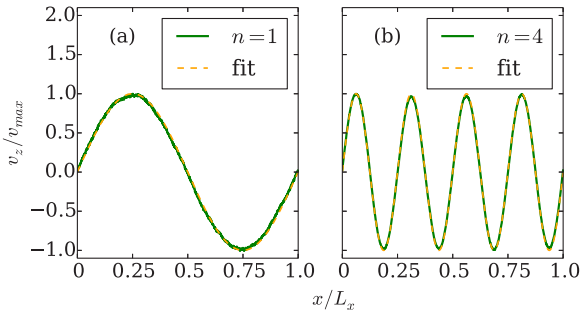

FIG. 1. Velocity profiles for different integer wave numbers and their analytical approximation (11). The statistical error is less than 1%.

TABLE III. Input parameters of the DPD solvent for the decay of sinusoidal waves.

Domain size ($L_x \times L_y \times L_z$)	$20 \times 20 \times 20$
Mass (m)	1
Temperature ($k_B T$)	1
Stochastic coefficient (σ)	3
Dissipative coefficient (γ)	$\sigma^2/(2k_B T)$
Repulsion coefficient (a_{ij})	18.75
Time step (dt)	0.01
Density (ρ)	4
Prerun length in time steps (N_{prerun})	4.8×10^4
Simulation length in time steps (N_{run})	1.2×10^4
Number of realization (N_{seed})	1000

A. Decay of sinusoidal waves

Considering the decay of sinusoidal waves allows us to asses the scale dependence not only of shear viscosity but also of other macroscopic transport coefficients such as bulk viscosity and isothermal speed of sound [25,26]. To analyze the evolution of dissipation of velocity modes in time one can consider the decay of the initial velocity perturbations. The dissipation rate of such perturbations can be determined for the different length scales. For convenience we impose initial velocity perturbations as sinusoidal waves at low Reynolds number. We opt to initialize sinusoidal waves of the velocity field in two directions, transverse and longitudinal with respect to the initial velocity field. For transverse perturbations the initial velocity field is given by

$$\boldsymbol{v}_\perp = \boldsymbol{v_r} + v_{\max}(k_z)\rho^2 \sin(k_z z)\hat{\boldsymbol{e}_x}, \tag{14}$$

where $\boldsymbol{v_r}$ is a random velocity field, and $\hat{\boldsymbol{e}_x}$ is the unit vector in the x direction. To generate the random velocity field we run simulations with zero initial conditions for N_{prerun} time steps. $k_z = 2\pi n_z/L_z$ is the wave number of interest. For the case of longitudinal perturbations the initial velocity field is

$$\boldsymbol{v}_\parallel = \boldsymbol{v_r} + v_{\max}(k_x)\rho^2 \sin(k_x x)\hat{\boldsymbol{e}_x}. \tag{15}$$

As a solution for longitudinal and transverse perturbations we expect to have

$$\boldsymbol{v}_\perp = v_{\max}(k_z)\rho^2 \sin(k_z z) f_\perp(k_z, t) \tag{16}$$

and

$$\boldsymbol{v}_\parallel = v_{\max}(k_x)\rho^2 \sin(k_x x) f_\parallel(k_x, t), \tag{17}$$

respectively. At the standard hydrodynamic regime (in the limit of long time and large length scale) $f_\perp(k_z,t)$ and $f_\parallel(k_z,t)$ have analytical expressions, which assume exponential decay. As shown in Fig. 3, the exponential approximation of such functions can result in additional errors in the estimation of macroscopic parameters. We run DPD simulations with initial conditions defined by Eqs. (14) and (15) for integer wave numbers $n_x, n_z = 1,4,11,21$. Simulation input parameters are given in Table III. For each integer wave number we perform independent simulations $N_{\text{seed}} = 1000$ and ensemble average the transient velocity profiles. Subsequently, for each averaged velocity profile we determine the decay of sinusoidal waves by assessing the functions $f_\perp(k_x,t)$ and $f_\parallel(k_x,t)$. Results are shown in Fig. 2 and are discussed below.

B. Stationary fluctuations

Now we consider the dissipation of random fluctuations of the velocity field without adding a mean flow. A convenient

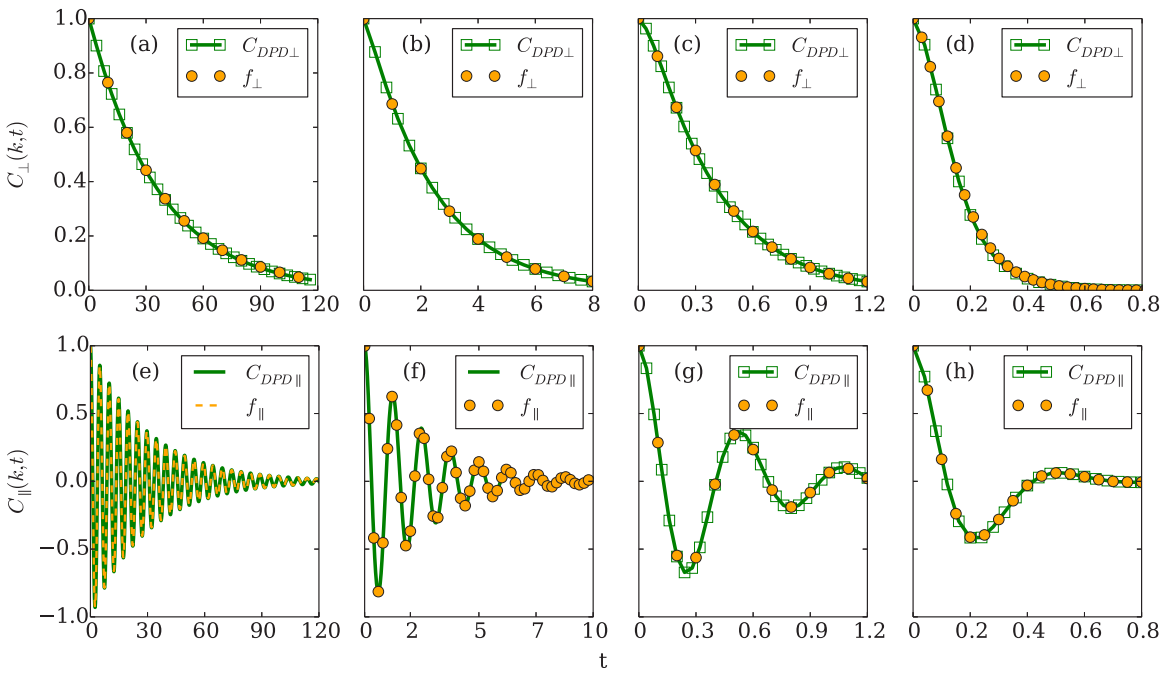

FIG. 2. Functions of decay of sinusoidal waves in parallel and perpendicular directions $f_\parallel$ and $f_\perp$ defined in Eqs. (16) and (17) compared with longitudinal $C_{\text{DPD}\parallel}$ and transverse $C_{\text{DPD}\perp}$ FTVACF measured in simulation. The comparison for different wave numbers is depicted from left to right as $n = 1,4,11,21$. We find a good agreement between the functions for different wave numbers.

way to derive the decay rate directly from the fluctuating velocity of the DPD solvent is to represent the random fluctuations of the particle velocity field as $\sum_{k_s} A_{k_s} f(k_s)$ where k_s is a length scale parameter. The dependence of macroscopic transport coefficients can be derived from the autocorrelation function of coefficients A_{k_s}. For zero mean flow, the common approach is to expand random fluctuations of the velocity field in space as Fourier series and to assess the dependency of macroscopic transport coefficients on the length scale from FTVACF. It is convenient to set

$$\hat{v}_l(k_m,t) = \sum_{j=1}^{N} v_{l,j}(m,t)\sin(m_j k_m). \tag{18}$$

For FTVACF $C(k_m,t)$ one can write

$$C(k_m,t) = \frac{\langle \hat{v}_l(k_m,t_0)\hat{v}_l(k_m,t_0+t)\rangle}{\delta \hat{v}_l^2(k_m,t)}. \tag{19}$$

Here $m = x,y,z$ and $l = x,y,z$ are direction indices and indicate the wave-number vector and velocity-vector components in the coordinate directions x,y,z, respectively. $m = l$ indicates longitudinal FTVACF with $C_\parallel(k,t)$, and $m \neq l$ indicates transverse FTVACF $C_\perp(k,t)$. $\delta\hat{v}_l^2(k_m,t)$ is the variance of the respective Fourier mode. It is possible to measure the functions $C_\perp(k,t)$ and $C_\parallel(k,t)$ from numerical simulations. We will denote FTVACF that are measured in simulations of a DPD solvent as $C_{\mathrm{DPD}\perp}(k,t)$ and $C_{\mathrm{DPD}\parallel}(k,t)$. To compare the functions $C_{\mathrm{DPD}\perp}(k,t)$ and $C_{\mathrm{DPD}\parallel}(k,t)$ with the decay of sinusoidal waves, we run DPD simulations with input parameters as given in Table III. After relaxation to stationary equilibrium, we transform the Lagrangian velocity distribution to a Eulerian field and then to Fourier space and measure FTVACF $C_{\mathrm{DPD}\perp}(k,t)$ and $C_{\mathrm{DPD}\parallel}(k,t)$. To minimize statistical error, we perform simulations with $N = 10^7$ time steps. Independent simulations are performed with different seeds $N_s = 32$ times to assess a statistical error. Figure 2 shows comparison of transverse $C_{\mathrm{DPD}\perp}(k,t)$ and longitudinal $C_{\mathrm{DPD}\parallel}(k,t)$ FTVACF exposed to the decay of an initial sinusoidal velocity field in transverse and longitudinal directions. FTVACF agrees with the decay of maximum velocities of sinusoidal waves from the previous subsection. There is neither numerical nor phenomenological difference between FTVACF and decay of sinusoidal waves. For convenience we choose to analyze longitudinal and transverse FTVACF in the remainder of the paper. In the following subsections we describe several methods of derivation of macroscopic transport coefficients from FTVACF. These methods will be compared in Sec. V.

C. Assumption of exponential decay

The behavior of a fluid on large scales can be described by the Navier-Stokes equations. An extension of the Navier-Stokes equations by a divergence of a random stress is able to capture many physical phenomena of thermal fluctuations on mesoscales such as multispecies mixing [27], diffusion enhancement and giant fluctuations [28,29], or the random walk of stationary shock [30]. Landau and Lifshitz first proposed this extension [31]. The velocity autocorrelation function is one of the main quantities to describe the statistical properties of the solvent. For the transverse and longitudinal FTVACF in case of LLNS we write [25]

$$C_{\mathrm{LLNS}\perp}(k,t) = e^{-k^2\frac{\eta_s}{\rho}t} \tag{20}$$

and

$$C_{\mathrm{LLNS}\parallel}(k,t) = e^{-k^2\Gamma t}\cos(\Theta k t) - \frac{k\Gamma}{\Theta}e^{-k^2\Gamma t}\sin(\Theta k t), \tag{21}$$

respectively, where

$$\Theta = \frac{\sqrt{4\,c_t^2 - k^2\Gamma^2}}{2}, \quad \Gamma = \left(1-\frac{1}{d}\right)\frac{\eta_s}{\rho} + \frac{1}{2}\frac{\eta_v}{\rho}, \tag{22}$$

and $d = 3$ is the number of dimensions. The DPD method is able to represent phenomena beyond the standard hydrodynamic limit and capture the mesoscopic hydrodynamics regime as well as N-particle Langevin dynamics [15,17]. To extend the analysis of collective properties of a DPD solvent to small scales we follow [17] and introduce the functions $\eta_s(k)$, $\eta_v(k)$, $c_t(k)$ instead of constant values of the macroscopic transport coefficients. The wave-number dependence in this case serves to describe the macroscopic properties of a DPD solvent on different wave numbers k. An accurate approximation of $C_{\mathrm{DPD}\parallel}(k,t)$ and $C_{\mathrm{DPD}\perp}(k,t)$ that are measured in the simulation allows us to estimate transport coefficients on different wave numbers k. To extend the functions $C_{\mathrm{LLNS}\perp}(k,t)$ and $C_{\mathrm{LLNS}\parallel}(k,t)$ to small scales one may consider wave-number dependent transport coefficients in Eqs. (20) and (21):

$$C_\perp(k,t) = e^{-k^2\frac{\eta_s(k)}{\rho}t} \tag{23}$$

and

$$C_\parallel(k,t) = e^{-k^2\Gamma(k)t}\cos[\Theta(k)kt] - \frac{k\Gamma(k)}{\Theta(k)}e^{-k^2\Gamma(k)t}\sin[\Theta(k)kt], \tag{24}$$

respectively, with

$$\Theta(k) = \frac{\sqrt{4\,c_t^2(k) - k^2\Gamma^2(k)}}{2}, \quad \Gamma(k) = \left(1-\frac{1}{d}\right)\frac{\eta_s(k)}{\rho} + \frac{1}{2}\frac{\eta_v(k)}{\rho}. \tag{25}$$

The FTVACF quantities $C_{\mathrm{DPD}\parallel}(k,t)$ and $C_{\mathrm{DPD}\perp}(k,t)$ that are measured from simulations can be approximated by Eqs. (23) and (24). From the result of the approximation one can derive the wave-number dependence of macroscopic transport coefficients $\eta_s(k)$, $\eta_v(k)$, $c_t(k)$. The results of the approximation for different wave numbers $n = 1,4,11,21$ are shown in Fig. 3. The results reveal that the approximation of FTVACF of a DPD solvent by the functions $C_\parallel(k,t)$ and $C_\perp(k,t)$ introduces approximation errors that affect the assessment of macroscopic transport coefficients. This error will be demonstrated and discussed in Sec. V.

D. Integral characteristics of FTVACF

Another approach to estimate shear viscosity is to integrate numerically FTVACF $C_{\mathrm{DPD}\perp}(k,t)$ in time. For transverse

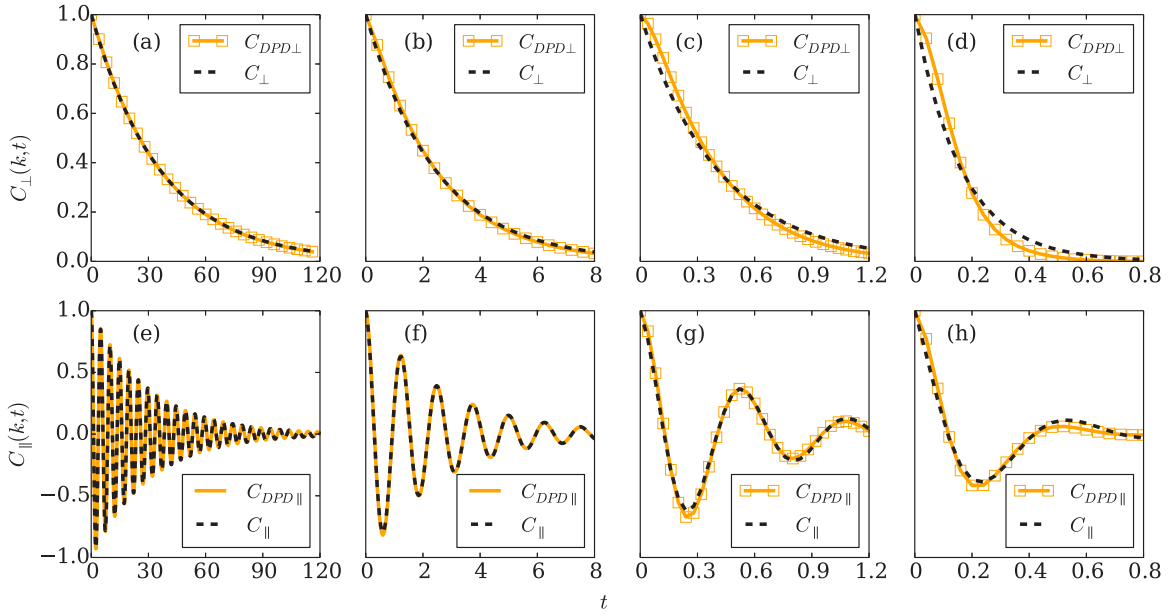

FIG. 3. FTVACF of DPD solvent $C_{\mathrm{DPD}\perp}$ and $C_{\mathrm{DPD}\parallel}$ which are measured from simulations compared with exponential approximations $C_\perp$ Eq. (23) and $C_\parallel$ Eq. (24). The comparison for different integer wave numbers is depicted (from left to right) as $n = 1,4,11,21$. We observe a deviation of the approximation functions and FTVACF of the DPD solvent for integer wave numbers $n \geqslant 11$.

FTVACF we write

$$\int_0^{t_1} C_{\mathrm{DPD}\perp}(k,t)dt = \int_0^{t_1} e^{-k^2\frac{\eta_s(k)}{\rho}t}dt \overset{t_1\to\infty}{=} \frac{\rho}{\eta_s(k)k^2}, \tag{26}$$

where t_1 is the maximum time difference for which we measure transverse and longitudinal FTVACF. The wave-number dependence of the shear viscosity $\eta_s(k)$ is given by

$$\eta_s(k) = \frac{\rho}{k^2}\left(\int_0^{t_1} C_{\mathrm{DPD}\perp}dt\right)^{-1}. \tag{27}$$

The longitudinal FTVACF depends on two transport coefficients and both isothermal speed of sound and bulk viscosity cannot be directly derived from integration of longitudinal FTVACF. A disadvantage of the method is related to finite time t_1. FTVACF is measured in the following way: during the simulation at every time step δt we measure the correlation between the instantaneous velocity $v(k,t_0+\delta t)$ in Fourier space and stored ones from the previous velocity field that consists of $N_v = t_1/\delta t$ elements. δt is a time step of FTVACF that could in principle be larger than the time step of the DPD computation dt. Computational cost of measuring modes of FTVACF directly relates to N_v. To minimize errors in the numerical evaluation of the integral (26) it is important to keep t_1 as large as possible. One way to decrease t_1 is to approximate $C_{\mathrm{DPD}\perp}(k,t)$ by some suitable function $g_\perp(k,t)$ and then compute the integral (26) for $t_1 = \infty$. Section IV F describes suitable choices for the function $g_\perp(k,t)$ in detail.

E. Fourier transform of the density autocorrelation functions

Equations (23) and (24) are derived from isothermal linearized LLNS equations which have macroscopic nature. Characteristics of DPD solvent $C_{\mathrm{DPD}\perp}(k,t)$ and $C_{\mathrm{DPD}\parallel}(k,t)$ might differ from Eqs. (23), (24), and (30) due to microscopic properties of a DPD solvent as well as truncation errors. For the shear mode one can compare the prediction of shear viscosity derived from $C_{\mathrm{DPD}\perp}(k,t)$ with the prediction derived from Kolmogorov flow. To estimate the accuracy of bulk viscosity and isothermal speed of sound derived from longitudinal FTVACF $C_{\mathrm{DPD}\parallel}(k,t)$ we consider Fourier transform of the density autocorrelation function (FTDACF). Unlike other particle methods such as SPH and SDPD the the DPD method does not model density field explicitly. Each particle of the DPD solvent has constant mass. The mass density of the DPD solvent can be introduced through the kernel approximation at every point of the DPD solvent. For simplicity we assume that the mass density is unity at the locations of DPD particles and introduce FTDACF similarly as FTVACF:

$$\hat{\rho}(k_m,t) = \sum_{j=1}^{N} \rho_j \sin(m_j k_m), \tag{28}$$

where $\rho_j = 4$ is a mass density of a DPD particle with index j. For FTDACF we write

$$C_{\mathrm{DPD}\rho}(k_m,t) = \frac{\langle\hat{\rho}(k_m,t_0)\hat{\rho}(k_m,t_0+t)\rangle}{\delta\hat{\rho}^2(k_m,t)}. \tag{29}$$

As mass density is a scalar we have only a single FTDACF component. Similarly to Eq. (24) we write

$$C_\rho(k,t) = e^{-k^2\Gamma(k)t}\cos[\Theta(k)kt] + \frac{k\Gamma(k)}{\Theta(k)}e^{-k^2\Gamma(k)t}\sin[\Theta(k)kt]. \tag{30}$$

In the following section we introduce the function $g_\parallel$ that may improve accuracy of prediction of bulk viscosity and isothermal speed of sound.

F. Nonexponential approximation of FTVACF modes

Figure 3 demonstrates that transverse and longitudinal FTVACF exhibit nonexponential behavior on small scales. Note that it has been established that the deviation from exponential decay on small scales is physically sound [14,19,20,32–35]. Such a deviation may be approximated by the introduction of a memory function. Consider the time correlation function $C(t)$. Its memory function can be defined as

$$\frac{\partial}{\partial t}C(t) = -\int_0^t dt'\phi(t')C(t-t'). \tag{31}$$

On the large time scales where fluid dynamics is described by the Navier-Stokes equations, the memory function coincides with the Dirac delta function. On small scales the memory function is usually approximated by some phenomenological model. Given such a model one can derive a closed approximation for FTVACF modes. We suggest another approach: instead of introducing a memory function one can introduce functions to approximate the FTVACF modes. To derive macroscopic transport coefficients of the DPD solvent from measured FTVACF $C_{\mathrm{DPD}\perp}(k,t)$ and $C_{\mathrm{DPD}\parallel}(k,t)$, we modify the exponential functions $C_\perp(k,t)$ and $C_\parallel(k,t)$. The functions are modified by introducing a parameter that allows us to further reduce the approximation error. The approximation function of transverse FTVACF is $g(k,t)_\perp$ and is defined as

$$g(k,t)_\perp = e^{-k^2 A_k \frac{t^2}{t+B_k}}. \tag{32}$$

The parameters $A_k > 0$ and $B_k > 0$ depend on k and are calibrated to predict FTVACF. A_k has the dimension of kinematic viscosity and B_k has the dimension of time. To derive the shear viscosity one can compute the integral of the function (32):

$$\eta_s(k) = \frac{\rho}{k^2}\left(\int_0^\infty e^{-k^2 A_k \frac{t^2}{t+B_k}}\, dt\right)^{-1}. \tag{33}$$

It is important to emphasize that with $t \gg B_k$ the function $g(k,t)_\perp$ corresponds to the exponential function $C_\perp(k,t)$, and $\eta_s(k) = \rho A_k$. When t and B_k have the same order one can represent the integral of the function $g(k,t)_\perp$ as

$$\int_0^\infty g(k,t)_\perp dt = B_k e^{2k^2 A_k/B_k} K_{-1}\left(\frac{k^2 A_k}{B_k}, \frac{k^2 A_k}{B_k}\right), \tag{34}$$

where $K_{-1}(\frac{A_k}{B_k}, \frac{A_k}{B_k}) = \int_1^\infty e^{-\frac{A_k}{B_k}(t+\frac{1}{t})}\, dt$ is an incomplete Bessel function. In this work we evaluate the integral $\int_0^\infty g(k,t)_\perp dt$ numerically. To fit longitudinal FTVACF and FTDACF we write

$$g(k,t)_\parallel = e^{-k^2 C_k \frac{t^2}{t+D_k}}\left[\cos(\Theta_k kt) - \frac{kC_k}{\Theta_k}\sin(\Theta_k kt)\right], \tag{35}$$

$$g(k,t)_\rho = e^{-k^2 C_k \frac{t^2}{t+D_k}}\left[\cos(\Theta_k kt) + \frac{kC_k}{\Theta_k}\sin(\Theta_k kt)\right]. \tag{36}$$

For sufficiently large time differences $t \gg D_k$ Eq. (35) reduces to Eq. (21). The isothermal speed of sound $c_t(k)$ and the coefficients C_k and D_k may be derived directly from the approximation with function $g_\parallel(k,t)$ of the longitudinal FTVACF $C_{\mathrm{DPD}\parallel}(k,t)$ that is measured from the computational experiment. The parameter C_k has the dimension of sound attenuation and D_k has the dimension of time. For sound attenuation

$$\Gamma(k) = \frac{1}{k^2}\left(\int_0^\infty e^{-k^2 C_k \frac{t^2}{t+D_k}} dt\right)^{-1}. \tag{37}$$

The bulk viscosity relates to sound attenuation in three dimensions as

$$\eta_v(k) = 2\rho\Gamma(k) - \tfrac{4}{3}\eta_s(k). \tag{38}$$

Figure 4 shows the approximation of transverse and longitudinal FTVACF with the functions $g(k,t)_\perp$ and $g(k,t)_\parallel$. $g(k,t)_\perp$ gives a good approximation to the nonexponential decay of $C(k,t)_{\mathrm{DPD}\perp}$. The longitudinal approximation $g(k,t)_\parallel$ slightly differs from $C(k,t)_{\mathrm{DPD}\parallel}$ for large wave numbers. However, it improves the results in comparison to the exponential approximation $C(k,t)_\parallel$. A similar result, however not demonstrated here, was observed for approximation of $C(k,t)_{\mathrm{DPD}\rho}$.

V. PREDICTIVE CAPABILITY OF NONEXPONENTIAL APPROXIMATIONS

In this section we compare the predictive capability of nonexponential approximations of macroscopic transport coefficients with exponential approximations in terms of the wave-number dependence of $\eta_s(k)$, $\eta_v(k)$, and $c_t(k)$. Specifically, we compare four different measures and approximations of $\eta_s(k)$: (1) exact evaluation of Kolmogorov flow described in Sec. III; (2) approximation of FTVACF $C_{\mathrm{DPD}\perp}(k,t)$ with exponential function $C_\perp(k,t)$ from Sec. IV C; (3) integration of $C_{\mathrm{DPD}\perp}(k,t)$ described in Sec. IV D; and (4) nonexponential approximation of $C_{\mathrm{DPD}\perp}(k,t)$ described in Sec. IV F.

We perform three-dimensional simulations using the input parameters given in Table III and assess the dependence of the shear viscosity on wave number. The results are shown in Fig. 5. Simulation lengths are chosen such as to achieve a statistical error in the estimation of shear viscosity of less than 1%. As reference $\eta_s(k)$ we consider the shear viscosity that has been derived from the analysis of Kolmogorov flow. The estimation error is computed as

$$E|_{\eta_s}(k) = 100\frac{\eta_s(k) - \eta_s|_{KF\perp}(k)}{\frac{1}{N_k}\sum_k \eta_s|_{KF\perp}(k)}, \tag{39}$$

where $\eta_s(k)$ is the shear viscosity given by one of the approximations above, and $\eta_s|_{KF\perp}(k)$ is the reference shear viscosity. We observe that the shear viscosity derived from the exponential approximation $C_\perp$ deviates from the reference. This deviation originates from the fact that the transverse FTVACF of a DPD solvent is nonexponential as shown in Fig. 3. The estimation of $\eta_s(k)$ directly from an integration of $C_{\mathrm{DPD}\perp}(k,t)$ agrees with the reference for large wave numbers and should be exact as $t_1 \to \infty$. However, due to finite time t_1 the numerical value is slightly smaller. In the simulation we choose the same $t_1 = \text{const.}$ for all wave numbers. For small wave numbers t_1 should be larger than the current value which leads to an overestimation according to Eq. (27). However, this overestimation does not invalidate our general observation. When the shear viscosity is estimated from the nonexponential approximation of FTVACF using Eq. (32) we obtain a much better agreement with the exact value. From an analysis of the longitudinal FTVACF one can assess

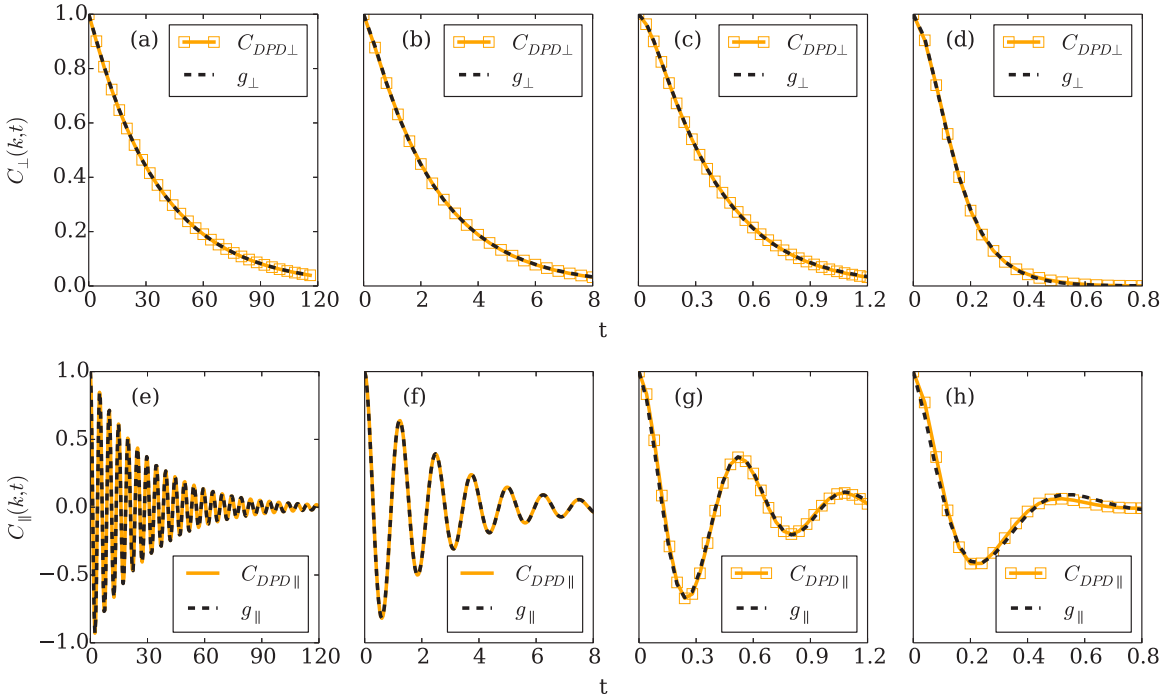

FIG. 4. FTVACF of DPD solvent $C_{\mathrm{DPD}\perp}$ and $C_{\mathrm{DPD}\parallel}$ which are measured in simulation compared with nonexponential approximations $g_\perp$ Eq. (32) and $g_\parallel$ Eq. (35). The comparison for different wave numbers is shown as $n = 1,4,11,21$ (from left to right).

the dependence on wave number of macroscopic transport coefficients such as the bulk viscosity $\eta_v(k)$ and the isothermal speed of sound $c_t(k)$. Aside from analytical estimations of such dependencies for the case of noninteracting DPD particles ($a_{ij} = 0$) in [17], no methods have been reported in literature so far for an estimation of $\eta_v(k)$ and $c_t(k)$ of a DPD solvent. For such purposes one can analyze the decay of sinusoidal longitudinal waves, which agrees, as has been shown in Fig. 2, with longitudinal FTVACF $C_{\mathrm{DPD}\parallel}(k,t)$ for low Reynolds numbers in the linear regime. In order to estimate the accuracy of estimates for $\eta_v(k)$ we compare four different methods that are based on the estimation of the bulk viscosity from longitudinal FTVACF $C_{\mathrm{DPD}\parallel}(k,t)$ and FTDACF $C_{\mathrm{DPD}\rho}(k,t)$: (1) approximation of FTVACF $C_{\mathrm{DPD}\parallel}(k,t)$ with exponential function $C_\parallel(k,t)$ from Sec. IV C; (2) nonexponential approximation of $C_{\mathrm{DPD}\parallel}(k,t)$ described in Sec. IV F; (3) approximation of FTDACF $C_{\mathrm{DPD}\rho}(k,t)$ with exponential function $C_\rho(k,t)$ from Sec. IV C; and (4) nonexponential approximation of $C_{\mathrm{DPD}\rho}(k,t)$ with function $g_\rho(k,t)$ described in Sec. IV F.

For assessment of $c_t(k)$ we consider four similar possibilities of using exponential and nonexponential approximations for $C_{\mathrm{DPD}\parallel}(k,t)$ and $C_{\mathrm{DPD}\rho}(k,t)$. Figure 6 shows the dependence of the bulk viscosity and the isothermal speed of sound on wave number that was estimated with the different methods. The statistical errors on both plots are smaller than the symbol size. Differences between approximations are quantified according to

$$D|_{c_t}(k) = c_t(k) - c_t|_{g\parallel}(k) \tag{40}$$

and

$$D|_{\eta_v}(k) = \eta_v(k) - \eta_v|_{g\parallel}(k). \tag{41}$$

For the assessment of the relative differences $D|_{c_t}(k)$ and $D|_{\eta_v}(k)$ in the approximations of $c_t(k)$ and $\eta_v(k)$ with the different methods we take the estimation derived from the nonexponential approximation of the longitudinal mode of FTVACF as reference. For the approximating error in the isothermal speed of sound, exponential $c_t(k)|_\parallel$ and nonexponential approximation $c_t(k)|_{g\parallel}$ from both FTVACF and FTDACF give similar results at small wave numbers. For large wave numbers the difference $D|_{c_t}$, the difference between estimation of $c_t(k)$ from FTVACF and FTDACF, is smaller for approximation with the nonexponential function. Moreover, in Fig. 4 we show that the nonexponential function $g(k,t)_\parallel$ improves the approximation of longitudinal FTVACF $C_{\mathrm{DPD}\parallel}(k,t)$ in comparison with the exponential function $C_\parallel$. For these reasons we consider results derived from the nonexponential approximation as more accurate for estimating $c_t(k)$.

The shear viscosity $\eta_s(k)$ and the isothermal speed of sound $c_t(k)$ are estimated directly from the transverse and the longitudinal FTVACF. However, to estimate the bulk viscosity from $C_{\mathrm{DPD}\parallel}(k,t)$ that is measured in simulations, one first needs to determine shear viscosity and isothermal speed of sound. Figure 6 shows the dependence of bulk viscosity, that is estimated with four different methods, on the wave number. We observe significant discrepancy between estimation of bulk viscosity from FTVACF and FTDACF. For the smallest wave number, difference is about 9% and it rises with larger wave numbers. The discrepancy is due to imperfections of the fitting function that is not able to incorporate the microscopic properties of the DPD solvent in the longitudinal direction. The improvement of the accuracy for the bulk viscosity prediction is a subject of future work. For both estimates the statistical error is smaller than the symbol size, quantitatively less than 1%. We show that the nonexponential approximations $g(k,t)_\perp$

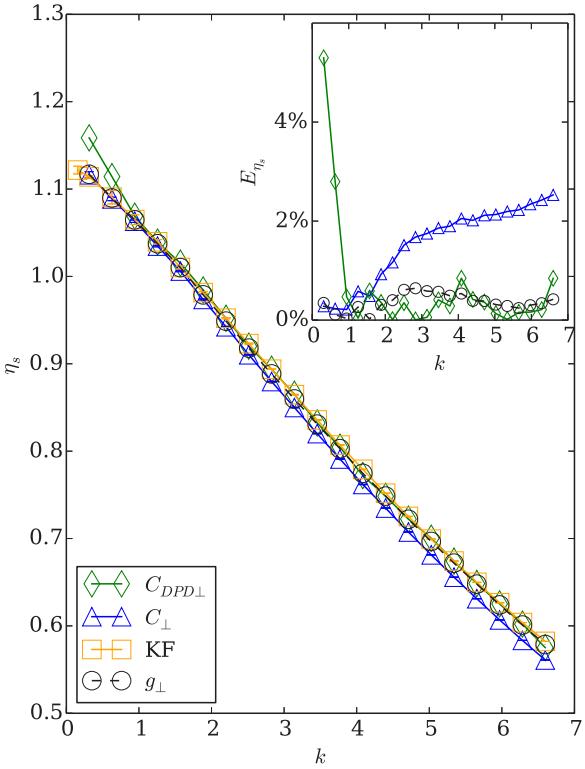

FIG. 5. Dependence of shear viscosity on wave number that is estimated with different methods. The exponential fit $C_\perp$ (blue lines with triangles) implies significant errors compared with the reference for Kolmogorov flow (orange line with squares) for large wave numbers. The large deviation at small wave numbers of the estimation that is derived by numerical integration of transverse FTVACF (green line with diamonds) can be explained by the limited time of measurement t_1. The black line with circles denotes the estimation from the exponential fit with function $g_\perp$. The error E_{η_s} is measured according to Eq. (39).

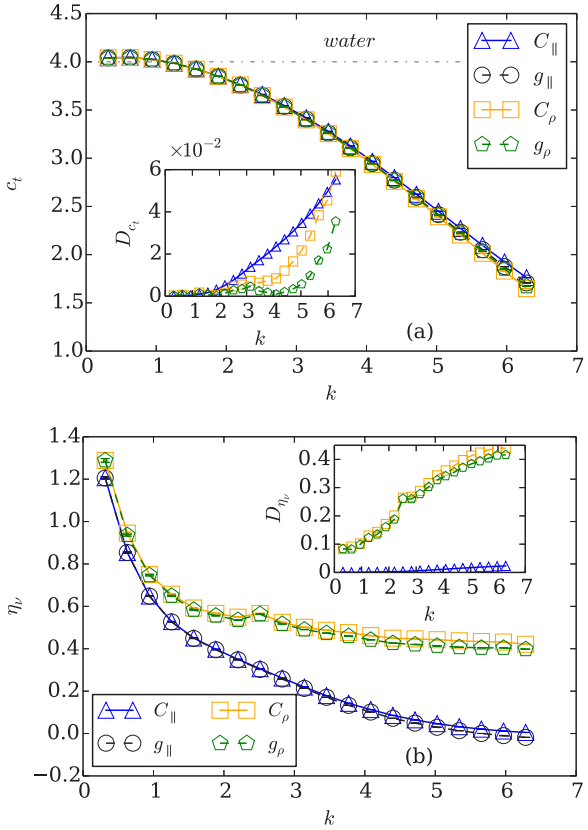

FIG. 6. Dependence of isothermal speed of sound and bulk viscosity on wave number, estimated with different methods. Differences between estimates D_{η_v} and D_{c_t} are computed from Eqs. (40) and (41).

and $g(k,t)_\parallel$ allow us to derive the wave-number dependence of macroscopic transport coefficients $c_t(k)$, $\eta_s(k)$, and $\eta_v(k)$. We also show that these predictions are more accurate than those derived from exponential approximations. Up to this point our attention was restricted to a single set of DPD input parameters. The following section is devoted to an extension of the approach to a wider range of DPD input parameters.

VI. NUMERICAL EXPERIMENTS

In this section we analyze the approximation capability of FTVACF with nonexponential functions $g_\perp(k,t)$ and $g_\parallel(k,t)$ for different sets of nondimensional DPD input parameters. We also estimate bulk viscosity and isothermal speed of sound for different Ω_0 (see Table I). To facilitate computations we shorten the domain size to $[L_x,L_y,L_z]=[10,10,10]$. We set the number density as $\rho=4$, temperature as $k_BT=1$, cutoff radius as $r_c=1$, and $\gamma=\frac{\sigma^2}{2k_BT}$. The number of time steps in the stationary regime is $N_t=4\times10^6$. For each set of input parameters we perform $N_{\text{seed}}=16$ independent simulations. The DPD input parameter k_BT is related to the nondimensional parameter Ω_0. For the kernel (9) the relation is

$$k_BT=\left(\frac{\pi m^{3/2}\rho r_c^4\sigma^2}{45\Omega_0}\right)^{\frac{2}{3}}. \tag{42}$$

A detailed derivation is provided in the Appendix. For the DPD input parameters of the previous section we have $\Omega_0=2.5$. In this section we take $\Omega_0=[0.1;0.3;1;5;10;20;50;100]$ with the corresponding k_BT. We choose a time-step size according to the relation $dt=0.01\sqrt{\frac{mr_c^2}{k_BT}}$ as in [36] for all cases except for $\Omega_0=[50;100]$ where $dt=0.01$. We vary the repulsive parameter of the DPD solvent $a_{ij}=[0;18.75k_BT]$. The particular choices of the repulsive potential are motivated by the fact that $a_{ij}=18.75k_BT$ is widely used for modeling water [2] and that for $a_{ij}=0$ analytical predictions of macroscopic transport coefficients in the classical hydrodynamics regime are possible [17].

A. Approximation error analysis

For each simulation we estimate the dependency $\eta_s(k)$ by three different methods: (i) from direct integration of $C_{\text{DPD}\perp}(k,t)$, (ii) by approximating $C_{\text{DPD}\perp}(k,t)$ with an exponential function $C_\perp(k,t)$, and (iii) by a nonexponential function $g_\perp(k,t)$. We take t_1 sufficiently large in order to obtain an accurate prediction of the shear viscosity dependence upon integration of $C_{\text{DPD}\perp}(k,t)$. We consider the shear viscosity obtained by integration of $C_{\text{DPD}\perp}(k,t)$ as reference. We

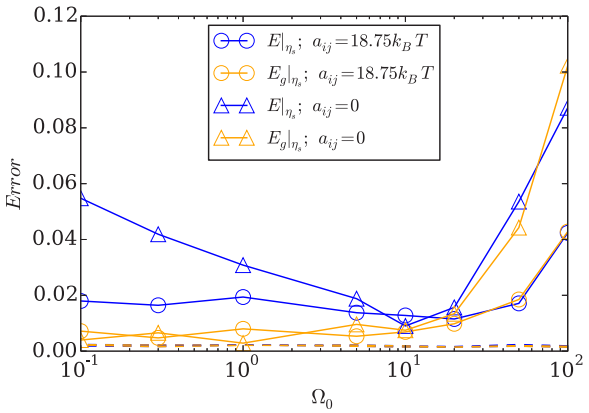

FIG. 7. Approximation errors (43) and (44) derived from different shear viscosity estimates for different values of Ω_0. As reference we integrate the transverse FTVACF measured in the simulation. Statistical errors are indicated with dashed lines.

estimate approximation errors for exponential and nonexponential approximations as

$$E|_{\eta_s} = \frac{\left[\sum_{k=2\pi/L}^{2\pi/r_c} \frac{r_c}{L}(\eta_s|_{\perp}(k) - \eta_s|_{\mathrm{DPD}\perp}(k))^2\right]^{\frac{1}{2}}}{\sum_{k=2\pi/L}^{2\pi/r_c} \eta_s|_{\mathrm{DPD}\perp}(k)} \tag{43}$$

and

$$E_g|_{\eta_s} = \frac{\left[\sum_{k=2\pi/L}^{2\pi/r_c} \frac{r_c}{L}(\eta_s|_{g\perp}(k) - \eta_s|_{\mathrm{DPD}\perp}(k))^2\right]^{\frac{1}{2}}}{\sum_{k=2\pi/L}^{2\pi/r_c} \eta_s|_{\mathrm{DPD}\perp}(k)}, \tag{44}$$

respectively. Figure 7 shows differences in the estimation of $\eta_s(k)$ by exponential and nonexponential functions. It demonstrates that for $\Omega_0 \leqslant 10$ the nonexponential function gives a better prediction than the exponential function. For $\Omega_0 \geqslant 10$ the prediction of $\eta_s(k)$ has a similar error. Large errors in the estimations of shear viscosity for the case $\Omega_0 \geqslant 20$ relate to the different shape of FTVACF for large Ω_0; consider the transverse FTVACF for the case of $\Omega_0 = 100$ shown in Fig. 8. As was mentioned in the previous section, no method to determine DPD solvent bulk viscosity and isothermal speed of sound except for that from FTVACF and FTDACF can be found in current literature. One can analyze the decay of sinusoidal waves for such purposes. However, this will result in the same $C_{\mathrm{DPD}\parallel}$ and it does not resolve the main issue of how to estimate $c_t(k)$ and $\eta_v(k)$ from longitudinal FTVACF and FTDACF. For that reason we do not estimate the approximation error for the isothermal speed of sound and bulk viscosity.

B. Simulation results

On the small scales of the DPD solvent shear and bulk viscosities are lower. With decreasing k the magnitudes of $\eta_s(k)$ and $\eta_v(k)$ increase until a certain plateau is reached. For the plateau, the dynamics of DPD particles can be described by classical hydrodynamics. To estimate the classical hydrodynamic level of viscosities it has been proposed to use the following expressions [15]:

$$\eta_s = \frac{\gamma\rho^2[\boldsymbol{r}w_d]_{\boldsymbol{r}}}{2d(d+2)} + \frac{dmk_BT}{2\gamma[\boldsymbol{r}w_d]_{\boldsymbol{r}}}, \tag{45}$$

and

$$\eta_v = \frac{\gamma\rho^2[\boldsymbol{r}w_d]_{\boldsymbol{r}}}{2d^2} + \frac{mk_BT}{\gamma[\boldsymbol{r}w_d]_{\boldsymbol{r}}}. \tag{46}$$

For nondimensional kinematic shear and bulk viscosity these expressions correspond to

$$\tilde{\nu} = \tfrac{1}{2} + a_2\Omega_0^2 \tag{47}$$

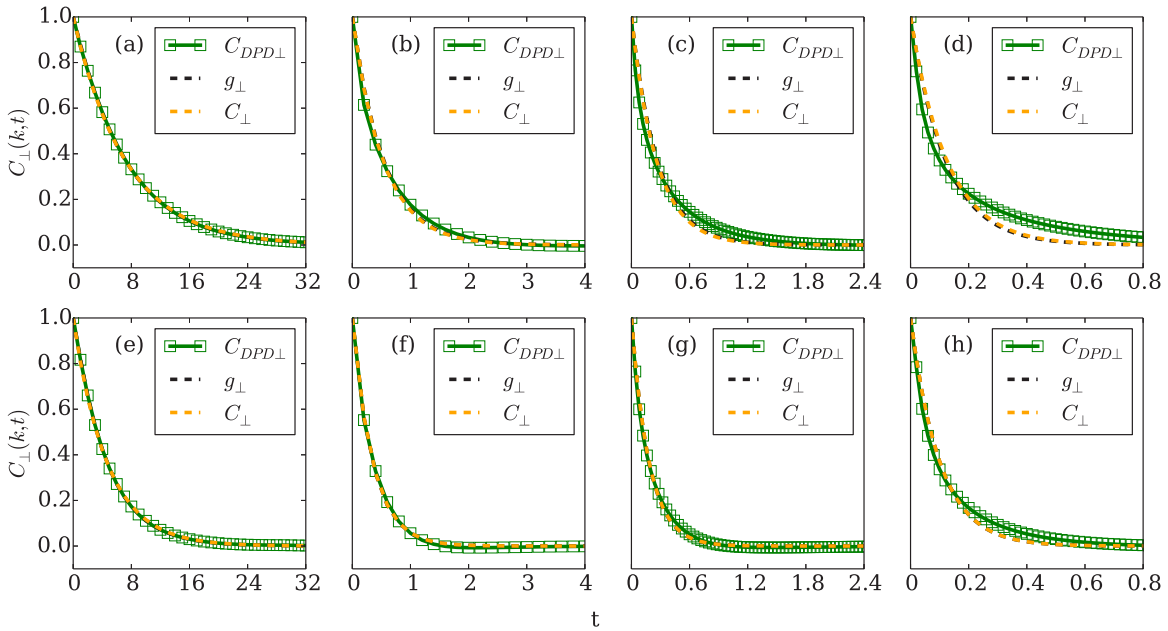

FIG. 8. Transverse FTVACF for $\Omega_0 = 100$ compared with exponential and nonexponential approximations for different wave numbers (from left to right) $n = 1,4,6,10$. Two cases considered: $a_{ij} = 0$ (top) and $a_{ij} = 18.75k_BT$ (bottom).

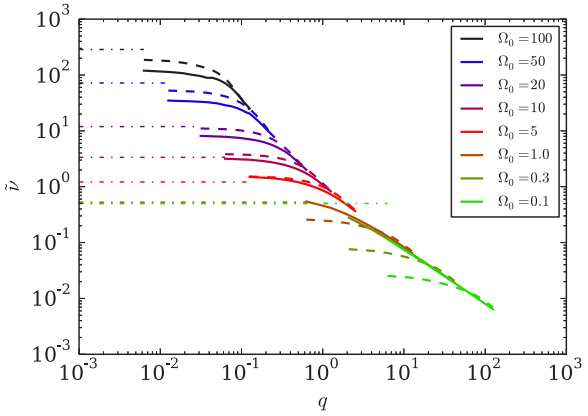

FIG. 9. Nondimensional kinematic shear viscosity $\tilde{\nu}$ dependence on nondimensional wave number $q = kl_0$ for different Ω_0 and different a_{ij}. Solid lines correspond to the case of $a_{ij} = 0$ and dashed lines correspond to $a_{ij} = 18.75k_BT$. Dash-dotted lines are estimations of the shear viscosity from Eq. (47) for the plateau values.

and

$$\tilde{\zeta} = \tfrac{1}{2} + \tfrac{1}{2}b_2\Omega_0^2, \tag{48}$$

respectively, where the coefficients a_2 and b_2 with kernel (9) are

$$b_2 = 3a_2 = \frac{3[\boldsymbol{r}w_D]_{\boldsymbol{r}}}{2(d+2)r_c^2[w_D]_{\boldsymbol{r}}} = \frac{3}{35}. \tag{49}$$

Figure 9 illustrates the dependence of the nondimensional kinematic shear viscosity on nondimensional wave number q. We compare simulations with $a_{ij} = 0$ and $18.75k_BT$ with the estimation of the kinematic shear viscosity from Eq. (47). The estimation (47) was derived for the case of $a_{ij} = 0$. We find that Eq. (47) may not give a good prediction for the plateau level of the kinematic shear viscosity even for the case without repulsive potential. For $\Omega_0 \geqslant 10$ Eq. (47) overestimates the shear viscosity measured from the simulation. For $10 > \Omega_0 \geqslant 1$ Eq. (47) underestimates shear viscosity measured from the simulation. For $\Omega_0 < 1$ the shear viscosity is far from the classical hydrodynamic limit due to the limitations in domain size, so that no definite conclusions can be drawn on the prediction (47) for the case of $a_{ij} = 0$. The kinematic shear viscosity measured from the simulation for the case of $a_{ij} = 18.75k_BT$ differs from that for $a_{ij} = 0$. For $\Omega_0 < 5$ the DPD solvent with repulsive potential has lower shear viscosity in comparison with the case without repulsive potential. For $\Omega_0 > 5$ the repulsive potential enhances shear viscosity.

Figure 10 shows the dependence of the nondimensional isothermal speed of sound on nondimensional wave number q. Two different values for the repulsive potential are considered, and two different estimation methods were used. For the case of zero repulsive potential and small Ω_0 the isothermal speed of sound remains constant. With increasing Ω_0 one can observe a deviation of $\tilde{c}_t(k)$ from the constant value. For the case of nonzero repulsive potential the estimation of the isothermal speed of sound with two different methods is similar for $\Omega_0 < 50$. The estimated isothermal speed of sound corresponds to the speed of sound in water $\tilde{c}_t = 4$ [2]. The small difference in the largest wave numbers between two methods may be due

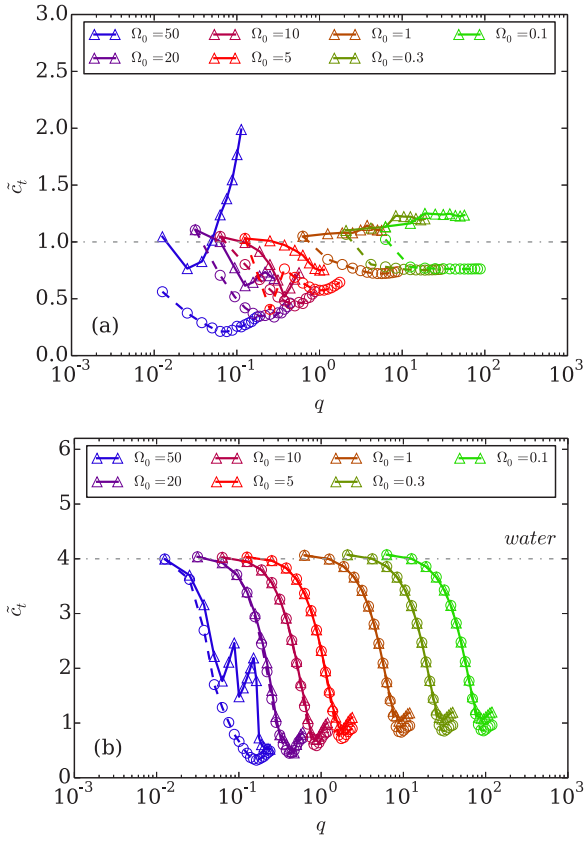

FIG. 10. Nondimensional isothermal speed of sound $\tilde{c}_t$ dependence on nondimensional wave numbers $q = kl_0$ for different Ω_0 and different $a_{ij} = 0$ (upper plot) and $a_{ij} = 18.75$ (lower plot). Solid lines with circles correspond to the measurements derived from analysis of longitudinal FTVACF and dashed lines with triangles correspond to measurements from FTDACF. The dash-dotted line is the nondimensional speed of sound in water on the lower plot [2] and analytical estimation for the case of zero repulsive potential $\tilde{c}_t = 1$ on the upper plot.

to truncation errors. The estimation of the isothermal speed of sound from longitudinal FTVACF and FTDACF differs for the case $a_{ij} = 0$ and is similar only for the largest wave number when $\Omega_0 \leqslant 20$. This may be related to the approximation error of FTVACF in the case of $a_{ij} = 0$. An approximation error was also found for large Ω_0. A further improvement of the estimation accuracy of $\tilde{c}_t(k)$ for the case of large Ω_0 as well as small a_{ij} is subject of future work.

In contrast to the estimation of the isothermal speed of sound we find that the kinematic bulk viscosity measured from simulations with different methods results in significant discrepancies for the case of both nonzero and zero repulsive potential on small scales and cannot be considered as accurate. For large scales the discrepancy between the two methods is smaller. We found a better agreement of the kinematic bulk viscosity with its estimation from Eq. (48) for large scales in comparison with measurements and predictions for kinematic shear viscosity. The results are given in Fig.11. Moreover, on large scales no differences in the bulk viscosity for $a_{ij} = 0$ and 18.75 was found for $\Omega_0 > 5$. When $\Omega_0 < 5$ we find that the bulk viscosity does not approach a plateau on the smallest

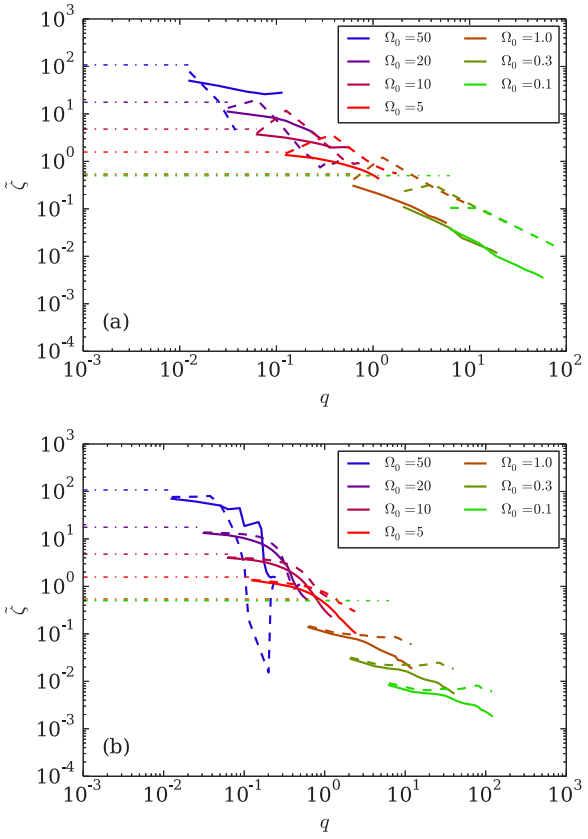

FIG. 11. Nondimensional kinematic bulk viscosity $\tilde{\eta}_v$ dependence on nondimensional wave number $q = kl_0$ for different Ω_0 and different $a_{ij} = 0$ (upper plot) and $a_{ij} = 18.75$ (lower plot). The legend is the same as that of Fig. 9. Dash-dotted lines are estimations of the shear viscosity from Eq. (48) for the plateau values. The solid line is the estimation from longitudinal FTVACF. The dashed line is the estimation from FTDACF.

measured wave number $k = \frac{2\pi}{L}$ and thus cannot be compared with the prediction.

VII. SUMMARY AND DISCUSSION

We start our analysis of a DPD solvent with the derivation of the dependence of the stationary shear viscosity on wave number with dynamic overlapping coefficient $\Omega_0 = 2.5$. For this purpose we use the Kolmogorov flow. Subsequently, we consider the decay of sinusoidal waves to estimate dynamic properties of shear viscosity. We show that the decay of sinusoidal waves for the case of parallel and perpendicular directions corresponds to longitudinal and transverse FTVACF. The dynamic overlapping is a nondimensional parameter that defines the dynamic regime of the DPD solvent [17]. For $\Omega_0 = 2.5$, the DPD solvent corresponds to the case considered in [10]. For the case of $\Omega_0 = 2.5$ we demonstrate the nonexponential character of transverse and longitudinal FTVACF. The estimation of stationary shear viscosity from the exponential approximation shows a significant deviation from the stationary shear viscosity, derived from an analysis of Kolmogorov flow. To fit both longitudinal and transverse FTVACF we propose nonexponential functions $g_\perp(k,t)$ and $g_\parallel(k,t)$, which recover exponential functions for small parameters B_k and D_k. We show that the shear viscosity which is estimated from an approximation of FTVACF modes with nonexponential functions agrees with the stationary shear viscosity computed for Kolmogorov flow. We use the same method to derive the dependence of other macroscopic transport coefficients, such as bulk viscosity and isothermal speed of sound, on wave number.

In order to assess the applicability limits of the approach, we perform simulations with different DPD input parameters. We show that the method of derivation of the shear viscosity from a nonexponential fit of FTVACF is suitable for a wide range of input parameters $\Omega_0 < 20$. The proposed method is more accurate than the derivation of macroscopic transport coefficients from exponential functions for $\Omega_0 \leqslant 10$ and gives the same approximation errors for $\Omega_0 > 10$. We assess the accuracy of the prediction of shear viscosity in the classical hydrodynamic limit Eqs. (47) and (48) that was proposed in [15] which matches neither the case of the DPD solvent without repulsive potential nor that with repulsive potential $a_{ij} = 18.75 k_B T$. In contrast, the prediction of the classical hydrodynamics limit of the bulk viscosity shows better agreement with the bulk viscosity measured from the simulation on the largest scale. The nondimensional isothermal speed of sound for the DPD solvent with repulsive potential is similar to that for waterlike fluid on large scales. In the case of zero repulsive potential the isothermal speed of sound corresponds to unity, the value that was derived from analysis [17].

The analyses described in the paper allow us to asses macroscopic transport properties on different scales. The estimation can help in coupling the DPD solvent with other mesoscale methods such as LLNS or SDPD. Moreover, for the case of $\Omega_0 < 20$ the analysis is accurate for shear viscosity on the small scale and may be useful to couple the DPD solvent with molecular dynamics. One may also assess the accuracy of the DPD solvent in representing phenomena beyond the standard hydrodynamic limit. Modes of FTVACF can be measured in the experiment and compared with the simulation of the DPD solvent and with simulations of molecular dynamics.

Introducing $g_\perp(k,t)$ and $g_\parallel(k,t)$ can be interpreted as an attempt to construct a surrogate model for the memory function of a DPD solvent. The analytical derivation of the exact memory function is tedious and not necessarily possible. However, an accurate approximation by a model of the memory function of the solvent allows us to predict the k dependence of the solvent *a priori*. For that purpose, it can be useful to consider the dependence of the fitting parameters A_k, B_k, C_k, D_k on different scale ranges, which may allow us to derive an empirical dependence of macroscopic transport coefficients of a DPD solvent on wave number from Eqs. (33) and (34).

We have considered so far only the classical DPD solvent. However, we believe that the analysis can be readily extended to measure the k dependence of macroscopic parameters for other variants of the DPD solvent, such as multibody DPD [37], energy-conserving DPD [38], and smoothed DPD (SDPD)[7]. For a classical DPD solvent we observe k dependence of macroscopic coefficients. This finding is in an agreement with the previous work on the topic [17]. On large scales, liquid behavior can be described by the Landau-Lifshitz

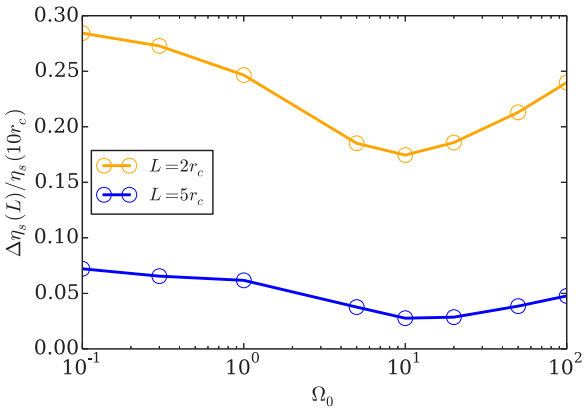

FIG. 12. Decreasing of viscosity for the case $a_{ij} = 18.75k_BT$ relative to the viscosity with wavelength $L = 10r_c$. In the legend $\eta_s(L)$ is a shear viscosity on wavelength L and relative error is estimated as $[\eta_s(L) - \eta_s(10r_c)]/\eta_s(10r_c)$. Different Ω_0 are considered.

Navier-Stokes equations, where viscosity does not depend on k. Beyond a certain scale, macroscopic parameters depend on k, and one has to account for such a dependence in the underlying model. One possibility is offered by the Lennard-Jones molecular dynamics (L-J MD) solvent. L-J MD has k-dependent macroscopic parameters and describes small-scale behavior of liquids [20]. DPD is a mesoscale model which has a wide range of applications and often is used to represent complex microfluidics phenomena where thermal fluctuations are important. We demonstrate the k dependency of macroscopic parameters of a DPD solvent which can be interpreted in two different ways: as a numerical artifact which one would like to avoid when DPD is used to model hydrodynamic length scales, or as an additional feature which allows us to model phenomena beyond the hydrodynamic limit. The described analysis can be applied in both cases, in order to modify the DPD solvent to minimize modeling artifacts, or to model small length scales beyond the hydrodynamic limit.

To minimize numerical artifacts when the length scales of interest are large enough and macroscopic parameters in liquids are known to be constant, one may consider other variants of the DPD solvent, such as SDPD. Another way to avoid the k dependence of macroscopic parameters may be to consider different kinds of DPD kernel functions. These studies are beyond the scope of the current paper.

On the other hand, the k dependence of macroscopic parameters is directly related to memory effects [20]. In recent studies the possibility of a physically motivated model for memory functions with a DPD solvent was demonstrated [39,40]. Using techniques described in the current paper, one can compare a classical DPD solvent with L-J MD simulations for different length scales and model memory effects of L-J MD according to such approaches. This allows us to increase the scale where a DPD model represents physical phenomena.

We observe no sharp critical limit beyond which DPD macroscopic parameters become constant. The evolution of macroscopic parameters losing their k dependence with increasing length scale is rather smooth. Figure 12 shows a comparison of relative viscosity differences of that at wavelength $L = 10r_c$ with that at wavelengths $L = 5r_c$ and $2r_c$. Different parameters Ω_0 are considered. One can observe that the viscosity at $L = 2r_c$ is smaller by 20–30% in comparison with the viscosity at wavelength $L = 10r_c$. Further investigations are needed to establish whether the k dependence of the viscosity affects the diffusion of colloids and polymers in DPD simulations.

The approach for assessing the isothermal speed of sound and the bulk viscosity may be improved for the case of zero repulsive potential by considering a more suitable approximation function for longitudinal FTVACF and FTDACF. For an accurate approximation function one would expect a similar prediction of macroscopic transport coefficients for both methods. With the nonexponential approximation we find a good agreement between predictions of the isothermal speed of sound derived from an analysis of FTVACF and FTDACF for the case of nonzero repulsive potential. The analyses show similar results for the prediction of bulk viscosity from FTVACF and FTDACF only for large length scales. The truncation error on small scales or on large scales can be estimated to improve the accuracy of the DPD solvent prediction, which is the subject of future work. For a DPD solvent with $\Omega_0 > 20$ new approximation functions which account for the long tail of DPD FTVACF should be introduced. In principle one can consider using machine-learning algorithms for the prediction of FTVACF in order to reduce the statistical error as well as the simulation length which is necessary for the derivation of macroscopic transport coefficients of particle methods.

ACKNOWLEDGMENTS

X.B. acknowledges George Em Karniadakis for both discussion and support for visiting Technische Universität München (TUM). The first author acknowledges travel support due to the TUM Graduate School. We thank the Munich Center of Advanced Computing for providing computational resources.

APPENDIX: RELATION OF DYNAMIC OVERLAP AND TEMPERATURE

We follow [17] and introduce the dynamic distance as

$$l_0 := t_0 v_0. \tag{A1}$$

Upon taking corresponding expressions for t_0 and v_0, one obtains

$$l_0 = \frac{1}{\omega_0}\sqrt{k_BT/m}. \tag{A2}$$

We insert the expressions for $\omega_0 := \frac{1}{d}\rho[\boldsymbol{r}w_D]_{\boldsymbol{r}}\gamma$ from Table I and $\gamma = \frac{\sigma^2}{2k_BT}$ from Table II into Eq. (A2) to get

$$l_0 = \frac{2k_BT}{\frac{1}{d}[\boldsymbol{r}w_D]_{\boldsymbol{r}}\rho\sigma^2}\sqrt{k_BT/m}. \tag{A3}$$

A typical DPD kernel is

$$w^D(r_{ij}) = [w^R(r_{ij})]^2 = \begin{cases} (1 - r_{ij})^{2\kappa}, & r_{ij} < r_c \\ 0, & r_{ij} \geqslant r_c \end{cases}, \quad \text{(A4)}$$

where κ is the parameter that controls kernel smoothness. Integration between zero and cutoff radius gives

$$[\boldsymbol{r} w_D]_{\boldsymbol{r}} = \int_0^{r_c} w_D(\boldsymbol{r}) d\boldsymbol{r} = \frac{8\pi r_c^3}{(2\kappa+1)(2\kappa+2)(2\kappa+3)}. \quad \text{(A5)}$$

We use $\kappa = 1$ and obtain

$$[\boldsymbol{r} w_D]_{\boldsymbol{r}} = \frac{8\pi r_c^3}{60}. \quad \text{(A6)}$$

Equation (A3) for the case of $d = 3$ dimensions becomes

$$l_0 = \frac{45 k_B T}{\pi r_c^3 \rho \sigma^2} \sqrt{k_B T / m}. \quad \text{(A7)}$$

Consequently, we obtain Eq. (42):

$$k_B T = \left(\frac{\pi m^{3/2} \rho r_c^3 l_0 \sigma^2}{45} \right)^{\frac{2}{3}}, \quad \text{(A8)}$$

where $\Omega_0 := \frac{r_c}{l_0}$. From that the relation between $k_B T$ and the nondimensional parameter Ω_0 follows as

$$k_B T = \left(\frac{\pi m^{3/2} \rho r_c^4 \sigma^2}{45 \Omega_0} \right)^{\frac{2}{3}}. \quad \text{(A9)}$$

[1] P. J. Hoogerbrugge and J. M. V. A. Koelman, Europhys. Lett. **19**, 155 (1992).
[2] R. D. Groot and P. B. Warren, J. Chem. Phys. **107**, 4423 (1997).
[3] D. A. Fedosov, B. Caswell, and G. E. Karniadakis, Biophys. J. **98**, 2215 (2010).
[4] E. S. Boek, P. V. Coveney, H. N. W. Lekkerkerker, and P. van der Schoot, Phys. Rev. E **55**, 3124 (1997).
[5] E. S. Boek, P. V. Coveney, and H. N. W. Lekkerkerker, J. Phys.: Condens. Matter **8**, 9509 (1996).
[6] E. E. Keaveny, I. V. Pivkin, M. Maxey, and G. E. Karniadakis, J. Chem. Phys. **123**, 104107 (2005).
[7] P. Espanol and M. Revenga, Phys. Rev. E **67**, 026705 (2003).
[8] J. Monaghan, Annu. Rev. Fluid Mech. **44**, 323 (2012).
[9] J. Kordilla, W. Pan, and A. Tartakovsky, J. Chem. Phys. **141**, 224112 (2014).
[10] X. Fan, N. Phan-Thien, N. T. Yong, X. Wu, and D. Xu, Phys. Fluids **15**, 11 (2003).
[11] J. A. Backer, Ph.D. thesis, University of Amsterdam, 2006.
[12] J. A. Backer, C. P. Lowe, H. C. J. Hoefsloot, and P. D. Iedema, J. Chem. Phys. **122**, 154503 (2005).
[13] D. A. Fedosov, G. E. Karniadakis, and B. Caswell, J. Chem. Phys. **132**, 144103 (2010).
[14] B. J. Palmer, Phys. Rev. E **49**, 359 (1994).
[15] C. A. Marsh, Ph.D. thesis, University of Oxford, 1998.
[16] C. A. Marsh, G. Backx, and M. H. Ernst, Phys. Rev. E **56**, 1676 (1997).
[17] M. Ripoll, M. H. Ernst, and P. Espanol, J. Chem. Phys. **115**, 7271 (2001).
[18] C.-C. Huang, G. Gompper, and R. G. Winkler, Phys. Rev. E **86**, 056711 (2012).
[19] B. Hess, J. Chem. Phys. **116**, 209 (2002).
[20] J. P. Boon and S. Yip, *Molecular Hydrodynamics* (Dover, New York, 1992).
[21] P. Espanol and P. Warren, Europhys. Lett. **30**, 191 (1995).
[22] S. Plimpton, J. Comput. Phys. **117**, 1 (1995).
[23] A. Vazquez-Quesada, M. Ellero, and P. Espanol, Phys. Rev. E **79**, 056707 (2009).
[24] H. A. Posch and W. G. Hoover, Physica A **240**, 286 (1997).
[25] G. De Fabritiis, M. Serrano, R. Delgado-Buscalioni, and P. V. Coveney, Phys. Rev. E **75**, 026307 (2007).
[26] X. Bian, Z. Li, and G. E. Karniadakis, J. Comput. Phys. **297**, 132 (2015).
[27] K. Balakrishnan, A. L. Garcia, A. Donev, and J. B. Bell, Phys. Rev. E **89**, 013017 (2014).
[28] A. Donev, J. B. Bell, A. de la Fuente, and A. L. Garcia, Phys. Rev. Lett. **106**, 204501 (2011).
[29] F. Balboa, J. B. Bell, R. Delgado-Buscalioni, A. Donev, T. G. Fai, B. E. Griffith, and C. S. Peskin, Multiscale Model. Simul. **10**, 1369 (2012).
[30] J. B. Bell, A. L. Garcia, and S. A. Williams, Phys. Rev. E **76**, 016708 (2007).
[31] L. D. Landau and E. M. Lifshitz, *Fluid Mechanics*, Course of Theoretical Physics Vol. 6 (Pergamon, London, 1959).
[32] B. J. Berne and G. D. Harp, *Advances in Chemical Physics* (Wiley, New York, 2007).
[33] B. J. Berne and R. Pecora, *Dynamic Light Scattering: With Applications to Chemistry, Biology, and Physics*, unabridged ed. (Dover, New York, 2000).
[34] P. Espanol and M. Serrano, Phys. Rev. E **59**, 6340 (1999).
[35] R. Zwanzig, Annu. Rev. Phys. Chem. **16**, 67 (1965).
[36] A. Boromand, S. Jamali, and J. M. Maia, Comput. Phys. Commun. **196**, 149 (2015).
[37] I. Pagonabarraga and D. Frenkel, J. Chem. Phys. **115**, 5015 (2001).
[38] Z. Li, Y.-H. Tang, H. Lei, B. Caswell, and G. E. Karniadakis, J. Comput. Phys. **265**, 113 (2014).
[39] Z. Li, X. Bian, B. Caswell, and G. E. Karniadakis, Soft Matter **10**, 8659 (2014).
[40] Z. Li, X. Bian, X. Li, and G. E. Karniadakis, J. Chem. Phys. **143**, 243128 (2015).